Crystal Growth, Structure, and Physical Properties of $LnCu_2(Al,Si)_5$ (Ln = La and Ce)

W. Adam Phelan,[†] Michael J. Kangas,[†] Brenton L. Drake,[†] Liang L. Zhao,[‡] Jiakui K. Wang,[‡] J. F. DiTusa,[§] Emilia Morosan,[‡] and Julia Y. Chan*[,†]

[†]Department of Chemistry, Louisiana State University, Baton Rouge, Louisiana 70803, United States
[‡]Department of Physics and Astronomy, Rice University, Houston, Texas 77005, United States
[§]Department of Physics and Astronomy, Louisiana State University, Baton Rouge, Louisiana 70803, United States

Ⓢ *Supporting Information*

ABSTRACT: $LnCu_2(Al,Si)_5$ (Ln = La and Ce) were synthesized and characterized. These compounds adopt the $SrAu_2Ga_5$ structure type and crystallize in the tetragonal space group $P4/mmm$ with unit cell dimensions of $a \approx 4.2$ Å and $c \approx 7.9$ Å. Herein, we report the structure as obtained from single crystal X-ray diffraction. Additionally, we report the magnetic susceptibility, magnetization, resistivity, and specific heat capacity data obtained for polycrystalline samples of $LnCu_2(Al,Si)_5$ (Ln = La and Ce).
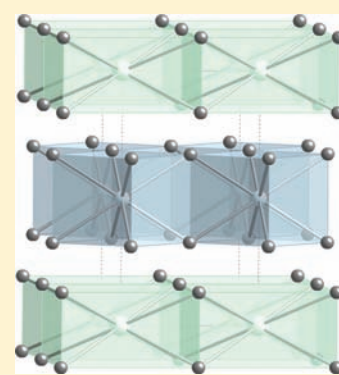
INTRODUCTION

The search for and understanding of materials that exhibit exotic behavior derived from complex, competing, or emergent phenomena begins with identifying the unifying characteristics of these materials. When searching for materials with competing ground states, such as Kondo screening and antiferromagnetism, where heavy electron metallic behavior and unconventional superconductivity can be found, it is obviously productive to explore Ce, Yb, and U containing compounds.[1−8] Heavy fermion behavior is commonly associated with Ce compounds and is characterized by an anomalously large Sommerfeld coefficient, γ, which parametrizes the electronic contribution to the specific heat capacity which is typically of the form $C = \gamma T + \beta T^3$. The overwhelming majority of Ce compounds contain Ce in a formal +3 valence state and order antiferromagnetically at low temperatures, whereas Yb containing phases more commonly exist in either the +2 and/or +3 oxidation states.

The unconventional superconductivity associated with quantum criticality discovered in the Ce_nMIn_{3n+2} (M = Co, Rh, or Ir; n = 1 or 2) phases has generated intense interest in finding novel highly correlated electron systems.[1,2,9] Further exploration and understanding of this system and its low-temperature behavior would be enhanced if an isostructural phase could be stabilized with M = Pd to investigate how the addition of one valence electron would perturb the ground state. Such an isostructural phase was not found; instead this research led to the discovery of a new compound. The antiferromagnetic (T_N = 5 K) heavy fermion compound, CePdGa₆ ($\gamma \approx 230$ mJ/mol K² mol as $T \rightarrow 0$ and 400 mJ/mol K² mol $T > T_N$),[4,10] was grown from excess Ga flux and crystallizes with a variant of the $SrAu_2Ga_5$ structure type.[11] Following this work, the structurally related intermetallic Ce_2PdGa_{12} was discovered and orders antiferromagnetically at 11 K, and shows moderately enhanced charge carrier mass with $\gamma > 70$ mJ/K² mol.[10] The discovery of these two new antiferromagnetic phases with enhanced mass behavior warranted the growth of both the Ni- and Cu-containing phases to investigate the effects of varying the transition metals on the structural stability and physical properties.[12,13] We found that the latter lanthanides form $\alpha - LnNiGa_4$ (Ln = Y, Gd−Yb) and $\beta - LnNi_{1-x}Ga_4$ (Ln = Tb−Er),[14] $SmCu_4Ga_8$,[15] and $Ln(Cu,Ga)_{12}$ (Ln = Y, Gd−Er, and Yb).[16] In any case, the Ni or Cu analogues were not found to adopt the $SrAu_2Ga_5$ structure type.[14,15,17,18]

Exploration of similar phase spaces using an Al flux resulted in the growth of $LaNi_{1+x}Al_{6-x}$[19] and more recently $CePd_{1-x}Al_{6-x}$.[20] The disorder in these compounds occurs on the same Wyckoff site that is observed to disorder in the parent phase, $SrAu_2Ga_5$. Density functional theory (DFT) calculations reveal the stabilization of $LaNi_{1+x}Al_{6-x}$ in this structure type may arise from the optimization of Al−Al and Al−Ni contacts in $LaNi_{1+x}Al_{6-x}$ and valence electron count of 19.68 electron/f.u.[19] This is in good agreement with CePdGa₆ ($\sim$ 21 e⁻/f.u.),[4] $SrAu_2Ga_5$ ($\sim$ 19 e⁻/f.u.),[11] and $CePd_{1-x}Al_{6-x}$ ($\sim$ 19.5 e⁻/f.u.)[20]

While working on compounds in the Ln−Cu−Al phase space (Ln = La and Ce) and searching for highly disordered Cu/Al compounds, we have serendipitously grown pseudoternaries of $LnCu_2(Al,Si)_5$ (Ln = La and Ce) which crystallize in the $SrAu_2Ga_5$ structure type. Herein we report the synthesis, magnetic, transport, and thermodynamic properties of the new compounds $LnCu_2(Al,Si)_5$ (Ln = La and Ce).

■ EXPERIMENTAL SECTION

Synthesis. *Flux Growth Synthesis.* Single crystals of Ce-$Cu_2(Al,Si)_5$ were grown in the presence of excess Al flux.[21] Ce (3N chunks), Cu (3N powder), Si (5N powder), and Al (5N pellets) were used as received (Alfa Aesar) and loaded into an alumina crucible with a reaction ratio of 1:2:0.1:10 for Ce:Cu:Si:Al, respectively. The crucible was placed into a fused silica tube along with silica wool which was used as a filtering medium, and the contents were evacuated (0.05−0.07 mmHg) and sealed. The charged vessel was loaded into a furnace and heated to a dwell temperature of 1200 °C for 72 h at 250 °C/h. Samples were slowly cooled to 1000 °C at a rate of 2 °C/h at which the cooling rate was doubled to 4 °C/h to a final dwell temperature of 720 °C, upon which the samples were centrifuged to separate crystals from the Al flux. Single crystals of $CeCu_2(Al,Si)_5$ were found growing off the surfaces of single crystals of $Ce(Cu,Si,Al)_4$.

The successful growth of $LaCu_2(Al,Si)_5$ was performed using the following conditions: La (3N chunks), Cu, Si, and Al were loaded into an alumina crucible with a reaction ratio of 1:2:1:5, respectively. The sample was heated to 1150 at 300 °C/h for 24 h. The sample was cooled to 720 °C at a cooling rate of 4 °C/h upon which the sample was centrifuged to remove the excess Al flux. Small (<0.5 mm × 0.5 mm × 0.05 mm) plate-shaped crystals were grown. Once again the $BaAl_4$ structure type, $La(Cu,Al,Si)_4$, impurity was observed. All of the above-mentioned reaction experiments were motivated by prior experiments where the incorporation of silicon from the silica wool was observed in single crystals that were grown while exploring the Ln−Cu−Al phase space. In all growths, silver-colored metallic crystals were retrieved via etching in NaOH (1−3 M) until excess aluminum was removed and subsequently cleaned with 10% HNO_3. These flux-free single crystals were observed to be air stable. The crystal morphology for both analogues is best described as plate-like.

Arc Melt Synthesis. Samples were prepared via arc-melting in an ultrapure Ar atmosphere employing Zr as an oxygen getter. The Ln, Cu, and Al constituent elements (same purities as mentioned above) were melted first, the resulting button was then turned over, and the Si pieces were then incorporated. Finally, each button was subsequently flipped and remelted three times to ensure homogeneity. Mass losses for the La and Ce analogues were 0.17% and 0.01%, respectively. Both samples were then annealed at 750 °C for 3 weeks.

Single Crystal X-ray Diffraction. Crystals of $LaCu_2(Al,Si)_5$ and $CeCu_2(Al,Si)_5$ obtained from flux growth were cut to suitable sizes for data collection (≤0.05 mm × 0.05 mm × 0.05 mm) and mounted onto separate glass fibers using epoxy. They were then mounted onto the goniometer of a Nonius KappaCCD X-ray diffractometer equipped with Mo Kα radiation (λ = 0.71073 Å). Crystallographic parameters for $LnCu_2(Al,Si)_5$ (Ln = La and Ce) are provided in Table 1. SIR97 was employed to give a starting model, SHELXL97 was used to refine the structural model, and the data were corrected using extinction coefficients and weighting schemes during the final stages of refinement.[22,23] Based on lattice parameters and the initial refinements, our starting structural model was found to be similar to $CePdGa_6$[4,10] with $LnCu_2(Al,Si)_5$ (Ln = La and Ce) crystallizing in the $SrAu_2Ga_5$ structure type.[11] However, refinement of the 2h (4mm) Wyckoff position assuming full main group element occupancy (Al), as observed in $CePdGa_6$, resulted in a model with an abnormally small anisotropic displacement parameter (ADP). Modeling the 2h Wyckoff position as having mixed occupancy of Cu and Al resulted in more well behaved ADP. This same type of disorder was observed for both $LnNi_{1+x}Al_{6-x}$[19] and $LnPd_{1+x}Al_{6-x}$.[20] Additionally, both Al and Si are found to be disordered on the 4i (2mm) Wyckoff site, resulting in a structural model that converged with small final difference residual

Table 1. Crystallographic Parameters for $LaCu_2(Al,Si)_5$ and $CeCu_2(Al,Si)_5$[a]

formula	$LaCu_2(Al,Si)_5$	$CeCu_2(Al,Si)_5$
a (Å)	4.221(1)	4.204(2)
c (Å)	7.916(2)	7.926(5)
V (Å^3)	141.04(6)	140.08(13)
Z	1	1
refined composition	$LaCu_{1.96(16)}Al_{4.04(16)}Si$	$CeCu_{1.95(10)}Al_{4.05(10)}Si$
cryst syst	tetragonal	tetragonal
space group	P4/mmm	P4/mmm
θ range (°)	2.55−34.97	2.55−37.04
μ (mm^{-1})	15.45	16.02
data collection		
measured reflns	3584	3584
indep reflns	228	226
reflections with $I > 2\sigma(I)$	227	226
R_{int}	0.020	0.017
h	−6 − 6	−6 − 6
k	−4 − 4	−4 − 4
l	−12 − 12	−12 − 10
refinement		
$^b R_1[F^2 > 2\sigma(F^2)]$	0.024	0.012
$^c wR_2(F^2)$	0.056	0.039
parameters	14	14
GOF	1.32	1.21
extinction	0.276(18)	0.192(5)
$\Delta\rho_{max}$ (eÅ^{-3})	1.98	0.76
$\Delta\rho_{min}$ (eÅ^{-3})	−2.45	−0.48

$^a w = 1/[\sigma^2(F_o^2) + (0.0344P)^2 + 0.1307P]$ and $w = 1/[\sigma^2(F_o^2)+(0.0181P)^2 + 0.2080P]$ for La and Ce, respectively. $^b R_1 = \sum||F_o| - |F_c||/\sum|F_o|$. $^c wR_2 = [\sum[w(F_o^2 - F_c^2)]/\sum[w(F_o^2)^2]]^{1/2}$.

Table 2. Selected Interatomic Distances (Å) for $LaCu_2(Al,Si)_5$ and $CeCu_2(Al,Si)_5$

	$LaCu_2(Al,Si)_5$	$CeCu_2(Al,Si)_5$
Ln−M^a rectangular prisms		
Ln−M (x8)	3.2083(7)	3.1944(14)
M−M (x4), c-axis	2.3533(19)	2.338(2)
M−M (x4), ab-plane	4.221(1)	4.204(2)
Cu−X^a rectangular prisms		
Cu−X (x8)	2.5133(8)	2.5110(11)
X−X (x4), c-axis	2.729(2)	2.747(2)
X−X (x4), ab-plane	2.9847(7)	2.9727(14)

^{a}M = Cu/Al and X = Al/Si.

peaks and well behaved ADPs. Selected interatomic distances are presented in Table 2, and atomic positions and ADPs are provided in Table 3. These tables reflect the structural models obtained after mixing the occupancy of the 2h and 4i positions. We note that the lattice parameter for the c-axis of $CeCu_2(Al,Si)_5$ is slightly larger than that of $LaCu_2(Al,Si)_5$. However, the volumes conform to the expected lanthanide contraction. Futhermore, multiple single crystal X-ray diffraction collections for both analogues showed this result was reproducible. The results for the most highly redundant data collection have been reported in Tables 1−3.

Powder X-ray Diffraction. Powder X-ray diffraction patterns were obtained using a Bruker AXS D8 Advance diffractometer (Cu Kα radiation, λ = 1.54056 Å) to determine the purity of the annealed polycrystalline samples. To more fully investigate the phase purities, high-resolution synchrotron powder diffraction data were collected at ambient temperatures using the 11-BM beamline (λ = 0.413262 Å) at the Advanced Photon Source located at Argonne National Laboratory.[24] Data points were collected over a 2θ range of 2°−50°

Table 3. Atomic Positions and ADPs for LnCu$_2$(Al,Si)$_5$ (Ln = La, Ce)

atom	Wyckoff position	x	y	z	occupancy	U_{eq} (Å^2)^a
La	1a	0	0	0	1.0	0.00656(19)
Cu	1b	0	0	1/2	1.0	0.083(2)
Cu/Al (M)	2h	1/2	1/2	0.14864(12)	0.482(8)/0.518(8)	0.0068(3)
Al/Si (X)	4i	0	1/2	0.32761(14)	0.75/0.25	0.0100(3)
Ce	1a	0	0	0	1.0	0.00615(10)
Cu	1b	0	0	1/2	1.0	0.00740(13)
Cu/Al (M)	2h	1/2	1/2	0.14752(8)	0.477(5)/0.523(5)	0.0064(2)
Al/Si (X)	4i	0	1/2	0.32670(10)	0.75/0.25	0.01003(16)

^{a}U$_{eq}$ is defined as $^1/_3$ of the trace of the orthogonalized U$_{ij}$ tensor.

with a step size of 0.001°. Rietveld refinements conducted using the GSAS and EXPGUI programs were employed to generate optimized models of the observed powder patterns for LnCu$_2$(Al,Si)$_5$ (Ln = La and Ce).[25,26] The refined models of LaCu$_2$(Al,Si)$_5$ and CeCu$_2$(Al,Si)$_5$ obtained from the single crystal X-ray diffraction experiments were employed as starting models in order to fit the data obtained from the 11-BM beamline. The histograms and the results of the Rietveld refinements are shown in Figure 1. For clarity, only a select 2θ range is
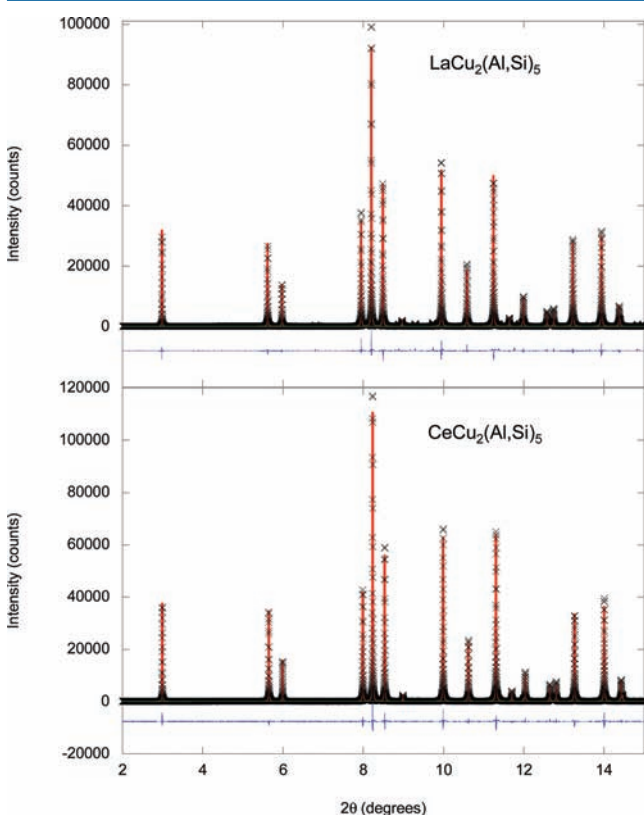

Figure 1. High-resolution X-ray diffraction powder patterns and Rietveld refinements of LaCu$_2$(Al,Si)$_5$ (above) and CeCu$_2$(Al,Si)$_5$ (below). The black cross, red fit line, green line, and blue line correspond to the observed data, calculated model, background fit, and difference curve, respectively.

shown. At low angles minor impurity peaks were resolved; however, attempts to model these impurity peaks were unsuccessful. The phase purity of LaCu$_2$(Al,Si)$_5$ was estimated to be greater than 95% by comparing the ratio of the most intense peak ($\sim$ 1300 counts) of the impurity phase to the most intense peak ($\sim$100 000 counts) of LaCu$_2$(Al,Si)$_5$. The results for phase purity of CeCu$_2$(Al,Si)$_5$ were determined to be roughly the same. The lattice parameters and the discrepancy factors obtained from refinement can be seen in Table 4.

Table 4. Crystallographic Parameters for LnCu$_2$(Al,Si)$_5$ (Ln = La and Ce) obtained from Rietveld Refinement

formula	LaCu$_2$(Al,Si)$_5$	CeCu$_2$(Al,Si)$_5$
a (Å)	4.218328(4)	4.195367(3)
c (Å)	7.933527(11)	7.913732(9)Å
V (Å^3)	141.1720(3)	139.291(1)
Z	1	1
refined composition	LaCu$_{2.04(26)}$Al$_{3.96(26)}$Si	CeCu$_{2.06(24)}$Al$_{3.94(24)}$Si
^{a}R$_p$	0.065	0.065
^{b}R$_{wp}$	0.091	0.080
^{c}R$_{exp}$	0.045	0.042
$^d\chi^2$	4.16	3.72

^{a}R$_p$ = $\sum|Y_o - Y_C|/\sum Y_o$. ^{b}R$_{wp}$ = $[M/\sum w(Y_o^2)]^{1/2}$. ^{c}R$_{exp}$ = Rwp/$(\chi^2)^{1/2}$. $^d\chi^2$ = $M/N_{obs} - N_{va}$.

These lattice parameters are slightly different from those obtained from single crystal X-ray diffraction. Because the Cu/Al occupancies of the 2h Wyckoff positions for both analogues are within error when comparing the results of the single crystal and powder diffraction models, certain experimental variables such as differing growth conditions, sample manipulation, and different experimental analysis (in-house single crystal X-ray diffraction compared with high-resolution synchrotron powder diffraction) could lead to these slight changes in the lattice parameters. Attempts to grow polycrystalline LnCu$_2$Al$_5$ on stoichiometry resulted in the formation of LnCuAl$_3$, again indicating Si is critical to phase stabilization of LnCu$_2$(Al,Si)$_5$ (Ln = La and Ce).

Elemental Analysis. Energy dispersive X-ray spectroscopy (EDS) experiments were conducted using a Hitachi S-3600N Variable Pressure scanning electron microscope equipped with an energy dispersive spectrometer. The accelerating voltage was 15 kV with a beam to sample distance of 15 mm. Four crystals, each of which were scanned three times resulting in 12 total compiled data points, were used to determine composition for CeCu$_2$(Al,Si)$_5$. For the LaCu$_2$(Al,Si)$_5$ sample, a small aggregate of single crystals was selected and a total to 10 data points collected on separate single crystals in the aggregate were used to determine composition. The results of the elemental analysis showed that Cu to Si ratio was 2 to 1 when normalized by the at.% Ln. The elemental composition for each compound were found to be La$_{1.00(2)}$Cu$_{1.95(6)}$Al$_{4.14(7)}$Si$_{0.97(3)}$ and Ce$_{1.00(2)}$Cu$_{1.96(4)}$Al$_{4.08(4)}$Si$_{0.95(3)}$. In light of these findings, the starting model obtained for single crystal X-ray diffraction for both analogues was inspected for mixed occupancy of Cu and Al in a fashion similar to the mixing observed in EuAu$_2$Ga$_5$ and SrAu$_2$Ga$_5$.[11] It is worth noting that Cu/Al and Al/Si mixing has been previously observed in Ln(Ag,Al,Si)$_2$ (Ln = Ce and Gd),[16] LnAlSi (Ln = La, Ce, Pr, Nd, Sm and Gd), LnAl$_2$Si$_2$ (Ln = Eu and Yb), and Ln$_2$Al$_3$Si$_2$ (Ln = Tb, Dy, Ho, Er, and Tm).[27]

Physical Properties. In light of a small amount of impurities (Ce(CuAl,Si)$_4$) on the single crystals after mechanical separation, polycrystalline samples of LaCu$_2$(Al,Si)$_5$ and CeCu$_2$(Al,Si)$_5$ were used for physical property measurements. Magnetic data were collected

using a Quantum Design Magnetic Property Measurement System (MPMS). The temperature-dependent susceptibility data were measured under field cooled (FC) conditions between 2.25 and 400 K for $CeCu_2(Al,Si)_5$ under an applied field of 1 T. Field-dependent magnetization data were measured between 5 and 20 K with applied fields up to 5 T. The electrical resistivity measurements for both samples were conducted on bar-shaped polycrystalline samples using a Quantum Design Physical Property Measurement System (PPMS). Specific heat capacity data for $LnCu_2(Al,Si)_5$ (Ln = La and Ce) were obtained down to liquid ^{3}He temperatures using the PPMS.

■ RESULTS AND DISCUSSION

Synthesis. As part of our motivation to synthesize the Cu analogue of $CePdGa_6$ with Al, single crystals of $CeCu_2(Al,Si)_5$ were grown. Silicon was initially introduced into the reaction from the silica wool filtering material at high temperatures. Subsequent growths were carried out with the following reaction ratios: (1) 1:2:0.1:10, (2) 1:2:0.5:10, and (3) 1:2:2:10 for Ce:Cu:Si:Al, which resulted in the growth of (1) $CeCu_2(Al,Si)_5$ and $Ce(Cu,Al,Si)_4$, (2) $CeCu_2(Al,Si)_5$ and $Ce(Cu,Al,Si)_4$, and (3) $Ce(Cu,Al,Si)_4$ for the aforementioned reaction ratios. The presence of both phases, $CeCu_2(Al,Si)_5$ and $Ce(Cu,Al,Si)_4$, was confirmed by both X-ray powder diffraction and single crystal X-ray diffraction. The stabilization of a phase adopting the $BaAl_4$ structure type may be expected due to the structural similarities between the $SrAu_2Ga_5$ and $BaAl_4$ structure types.[11,19] Attempts were made to mechanically separate the crystal morphologies. $CeCu_2(Al,Si)_5$ crystals grow as thin plates protruding from the surface of the $Ce(Cu,Al,Si)_4$ impurity. Small fragments of pure $CeCu_2(Al,Si)_5$ can be easily cleaved for single crystal X-ray diffraction. The mechanical separation of larger fragments for physical property measurements resulted in small amounts of the impurity phase remaining on the small single crystals of $CeCu_2(Al,Si)_5$.

Multiple attempts to grow the La analogue were completed with similar synthetic conditions used for the growth of $CeCu_2(Al,Si)_5$. Under these conditions, only $La(Cu,Si,Al)_4$ formed. The growth of $LaCu_2(Al,Si)_5$ was realized with stoichiometric flux growth conditions. Small (<0.5 mm^3) crystals were grown. Once again the $BaAl_4$ structure type, $La(Cu,Al,Si)_4$, impurity was also observed. In light of the presence of $Ln(Cu,Al,Si)_4$ (Ln = La and Ce) remaining on the small single crystals of $LnCu_2(Al,Si)_5$ (Ln = La and Ce) cleaved for physical property measurements and the inability to avoid the impurity phases, samples were prepared via arc-melting. X-ray powder diffraction patterns obtained from preannealed polycrystalline samples again indicated the presence of both $LnCu_2(Al,Si)_5$ (Ln = La and Ce) and $Ln(Cu,Si,Al)_4$ (Ln = La and Ce) impurities. Subsequent annealing resulted in >95% $LnCu_2(Al,Si)_5$ (Ln = La and Ce), suitable for physical property measurements.

Structure. The $SrAu_2Ga_5$ structure type has been shown to crystallize with a range of compositions that more closely resemble the general formula $LnM_{2-x}X_{5+x}$ where x can have values up to 1 when M = Pd and X = Ga.[4,11,19,20] Herein, $CeCu_2(Al,Si)_5$ will be discussed as the general structural model for both analogues, $LaCu_2(Al,Si)_5$ and $CeCu_2(Al,Si)_5$. The pseudoternary $CeCu_2(Al,Si)_5$, as shown in Figure 2, crystallizes in the $P4/mmm$ space group (no. 123) with lattice parameters of a = 4.204(2) Å and c = 7.926(5) Å, and the Ce, Cu, M, and X (M = Al/Cu and X = Al/Si) atoms occupying the $1a$, $1b$, $2h$, and $4i$ Wyckoff position, respectively. The structure can be best described as a stacking of rectangular prisms in alternating face/edge sharing arrangements rotated by 45° with respect to the
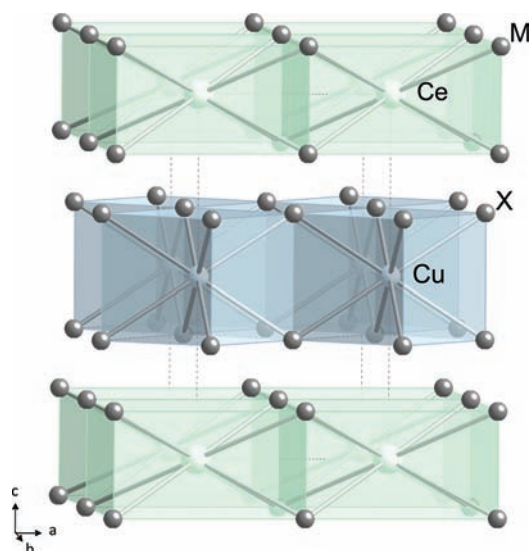

Figure 2. Crystal structure of $CeCu_2(Al,Si)_5$ is shown. Ce $(1a)$ atoms are represented with large light green spheres, Cu $(1b)$ atoms are denoted as medium light blue spheres, Al/Cu $(2h)$ atoms are denoted as M in small gray spheres, and Al/Si $(4i)$ atoms are denoted as X in small gray spheres. Dashed lines show the unit cell. The local 8 coordinate Ce environment is shown as a light green translucent rectangular prism with the 8 coordinate Cu local environments depicted as a translucent light blue rectangular prism.

other along the crystallographic c direction. The local environment of Ce $(1a)$ can be described as a face-sharing 8-coordinate rectangular prismatic environment ($CeM_{8/4}$, M = Cu and Al) where the local environment of Cu $(1b)$ can be described similarly as an edge-sharing rectangular prismatic environment ($CuX_{8/2}$, X = Al and Si).

In $SrAu_2Ga_5$ the $2h$ position is equally occupied by Ga and Au.[11] In a similar fashion we observe a nearly equal distribution of Cu and Al atoms on this position in $CeCu_2(Al,Si)_5$. Additional disorder was observed with Al and Si jointly occupying the $4i$ Wyckoff position. It is worthwhile to note that several synthetic attempts were made to grow Si free single crystals, all of which resulted in the growth of undesired phases. Both the $2h$ and $4i$ positions were checked for Si occupancy, but only mixing the occupancy of the $4i$ position with Si led to a stable structural model. It is difficult to refine structural models as obtained from X-ray diffraction, and obtain quantitative data relating to the chemical composition when constituents differ by only one atomic number (Si and Al). Therefore, the model was adjusted to reflect the composition of Si that resulted from EDS measurements; Cu was refined separately from the EDS results and independently reflected the values obtained from the EDS experiments. The final model resulted in a composition that was consistent with the elemental composition found by EDS. Ce to M (M = Cu/Al) distances agree well with other compounds that share a similar disorder of Cu and Al mixing. Ce−Cu/Al distances in $CeCu_2(Al,Si)_5$ of 3.1944(14) Å agree well with previously reported distances observed in $Ce(Cu,Al)_{12}$ and $CeCuAl_3$ of 3.2427(10) Å and 3.245(12) Å, respectively.[18,28] Cu−Al/Si distances in the title phase of 2.5110(11) Å agree well with distance found in related CuSi and CuAl containing phases [$Ce(Cu,Al)_{12}$ − 2.6972(7) Å, $CeCu_2Al_3$ − 2.5893(1) Å, $CeCu_2Si_2$ − 2.415, and CeCuSi − 2.4479(8) Å].[18,29−31]

Physical Properties. The temperature-dependent magnetic susceptibility of $CeCu_2(Al,Si)_5$ in a field of 1 T is shown in Figure 3. The modified Curie–Weiss equation was used to fit

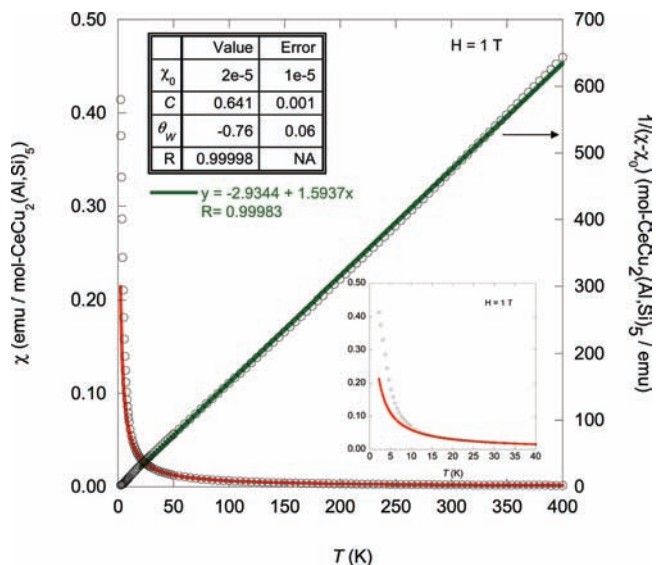**Figure 3.** Magnetic susceptibility, $\chi = M/H$ (emu/mol), of $CeCu_2(Al,Si)_5$ as a function of temperature measured under an applied field of 1 T is shown on the left axis, and inverse magnetic susceptibility, $1/\chi - \chi_0 = H/M$ (mol/emu), as a function of temperature is shown on the right axis. The χ_0, C, and θ_W parameters obtained from a modified Curie–Weiss fit to the susceptibility can be viewed in the upper inset of this figure. A graph comparing the Curie–Weiss fit to magnetic susceptibility can be seen in the lower right inset.

the magnetic susceptibility data from 20–400 K where $\chi(T) = \chi_0 + C/(T - \theta_W)$, C represents the Curie constant, θ_W is the Weiss temperature, and χ_0 represents the temperature-independent contributions to the magnetic susceptibility due to the Pauli paramagnetism and Larmor diamagnetism. The χ_0, C, and θ_W parameters obtained from this fit can be viewed in the inset table of Figure 3. These terms were used to generate the red line to extrapolate the Curie–Weiss form to lower temperatures for comparison to the magnetic susceptibility. The inset in Figure 3 shows that the data diverge from this form below 10 K. Furthermore, the magnetic susceptibility data deviate to higher values compared to the red curve, which is indicative of ferromagnetic correlations between magnetic moments. The χ_0 value obtained from the modified Curie–Weiss fit was subtracted from the raw magnetic susceptibility data and the inverse of $\chi - \chi_0$ is plotted on the right axis of Figure 3. A linear fit to these data from 20 to 400 K was performed in an attempt to extract more accurate C and θ_W values. The effective moments obtained from C were compared to the calculated values using $\mu_{eff} = g_J[J(J + 1)]^{1/2}$. We note that $CeCu_2(Al,Si)_5$ displays paramagnetic behavior down to 2.25 K and Curie–Weiss behavior above 20 K. The magnetic moment of 2.24(1) μ_B/mol Ce is somewhat lower than the expected moment of 2.54 μ_B/mol for a free Ce^{3+} ion. The observation of a somewhat smaller effective moment in $CeCu_2(Al,Si)_5$ was also observed for the related phase, $CePd_{1+x}Al_{6-5}$.[20] A positive Weiss constant, $\theta_W = 1.8(4)$ K, indicates weak ferromagnetic interactions in contrast to the Weiss temperature that results from the fitting procedure above. This indicates that the Weiss temperature is small and that our fitting of a Curie–Weiss form to the susceptibility does not result in an accurate

determination of the Weiss temperature. Therefore, we have scaled the field-dependent magnetization data to more accurately determine the θ_W as presented below.

The field-dependent magnetization up to 5 T at 5, 7, 9, 11, 15, and 20 K ia presented in Figure 4 for $CeCu_2(Al,Si)_5$. The

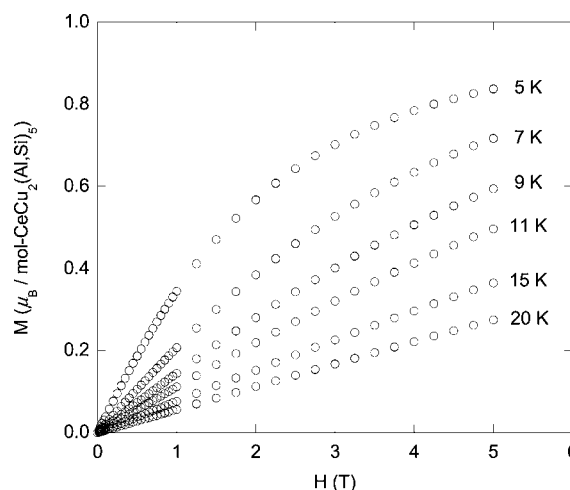**Figure 4.** Magnetization (M) of $CeCu_2(Al,Si)_5$ as a function of applied field (H) at 5, 7, 9, 11, 15, and 20 K.

magnetization data above 10 K are linear and show no sign of saturation whereas the data at 5, 7, and 9 K show a tendency toward saturation at high fields as expected for a paramagnet. Figure 5a and b show the field-dependent magnetization curves vs H/T and $H/(T - 2$ K$)$, respectively. As can be seen in Figure 5b, the data overlap and scale nicely when 2 K is subtracted from the sample temperatures. This again is suggestive of weak ferromagnetic correlations between the magnetic moments and reinforces the positive Weiss temperature, $\theta_W \approx 2$ K, obtained from Curie–Weiss fits of $\chi - \chi_0$.

The magnetocaloric effect is a promising refrigeration technology that utilizes the changes in magnetic entropy when a magnetic field is applied.[32] The magnetic entropy change can be approximated from a series of magnetic isotherms with $\Delta S_m = \Sigma_i(M_{i+1} - M_i)/(T_{i+1} - T_i)\Delta H_i$, where M_i and M_{i+1} are magnetizations at temperatures T_i and T_{i+1}, respectively.[33] $CeCu_2(Al,Si)_5$ shows a modest ΔS_m of -5 J/kg K at 5 K for a field change of 0–5 T and decreases with increasing temperature as expected for a paramagnet. For comparison, a common magnetocaloric material for this temperature region is $Gd_3Ga_5O_{12}$ which shows a ΔS_m of -24 J/kg K under similar conditions.[34]

The electrical resistivity as a function of temperature for $LnCu_2(Al,Si)_5$ (Ln = La and Ce) is shown in Figure 6. Metallic behavior is observed down to 2 K for both analogues. The resistivity of most metals is linear in temperature for $T > \theta_D$, where θ_D is the Debye temperature and is an estimate of highest frequency phonon modes. The high temperature resistivity is roughly linear in temperature down to ~50 K, which is indicative of a small Debye temperature (see below). The resistivity of $LaCu_2(Al,Si)_5$ at low T approaches a constant value indicating the reduction of phonon scattering and signaling the dominance of simple impurity and defect scattering. By comparison, $CeCu_2(Al,Si)_5$ displays a much more temperature-dependent resistivity. The differences with the resistivity of $LaCu_2(Al,Si)_5$ indicate that conduction electron/Ce f-electron scattering is likely cause. The resistivity
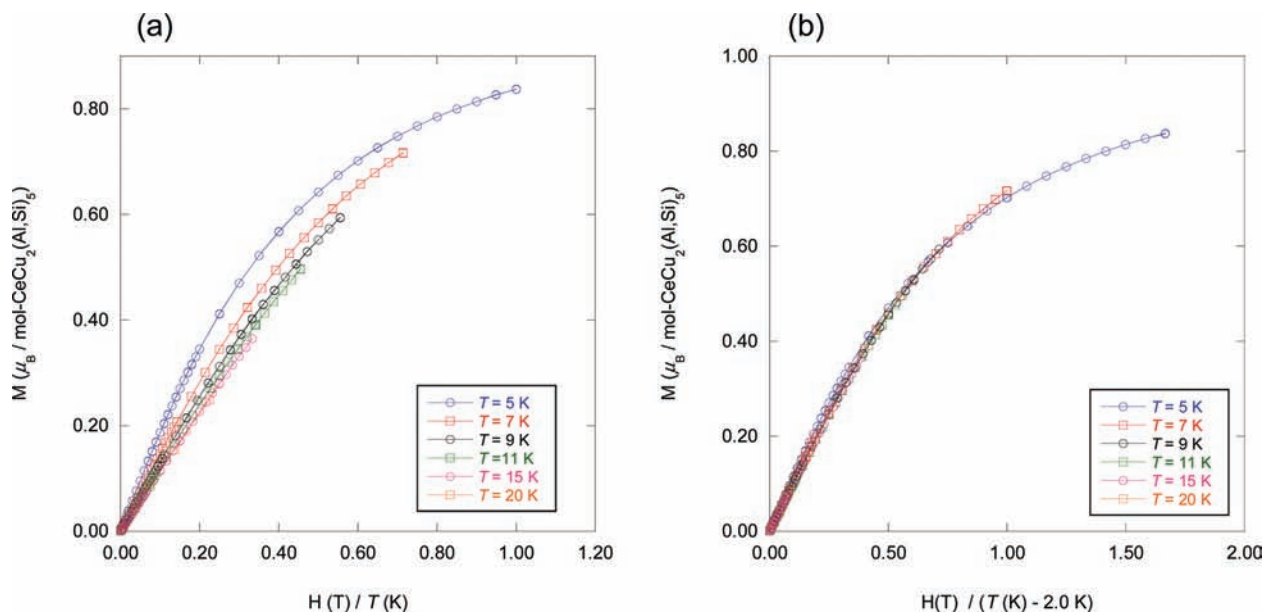
Figure 5. Magnetization (M) curves vs field divided by temperature (H/T) (a) and M vs H/(T − 2 K) to demonstrate scaling of the magnetization data (b).
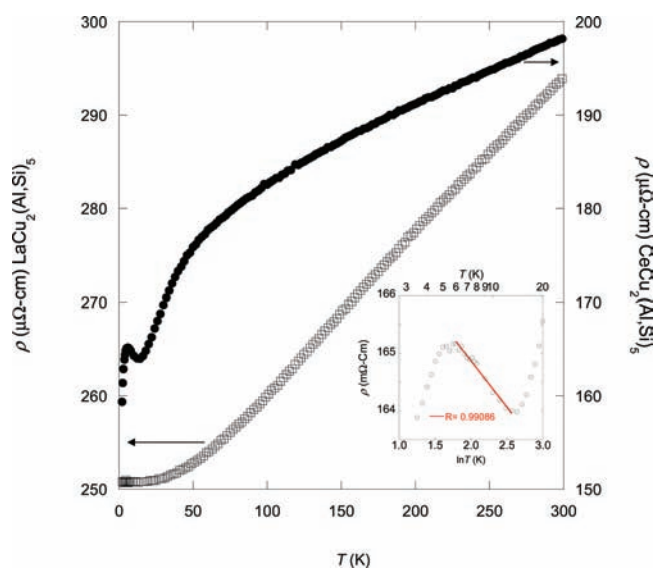

Figure 6. Temperature-dependent electrical resistivity (ρ) for LnCu$_2$(Al,Si)$_5$ (Ln = La and Ce). The inset shows a linear fit of ρ vs ln$T$ for CeCu$_2$(Al,Si)$_5$ from 6 to 13 K.

Figure 7. Heat capacity (C_p) for CeCu$_2$(Al,Si)$_5$ and LaCu$_2$(Al,Si)$_5$ as a function of temperature (T).

between 2 K and higher is similar to the behavior observed for CeMg$_3$,[35] Ce$_3$Ni$_2$Ge$_7$,[36] Ce$_2$Ni$_3$Ge$_5$,[36] and Ce$_3$Ni$_7$As$_5$,[37] and can be attributed to the interplay between the Kondo effect and crystalline electric field effects. Between 5 and 14 K a decreasing ρ with T is observed and when plotted in the inset of Figure 6, ρ as a function of ln$T$ displays linearity indicating a Kondo mechanism, although the T-range is limited (6 K < T < 13 K). The peak in resistivity data for CeCu$_2$(Al,Si)$_5$ around 5 K and a sudden drop in resistivity are likely related to the onset of a magnetic transition where the alignment of the magnetic moments reduces the spin disorder scattering.

The specific heat capacity (C_p) of LnCu$_2$(Al,Si)$_5$ (Ln = La and Ce) is shown in Figure 7. A magnetic contribution in C_p of CeCu$_2$(Al,Si)$_5$ as signaled by the deviation from the heat capacity of LaCu$_2$(Al,Si)$_5$, is observed below 10 K. This is

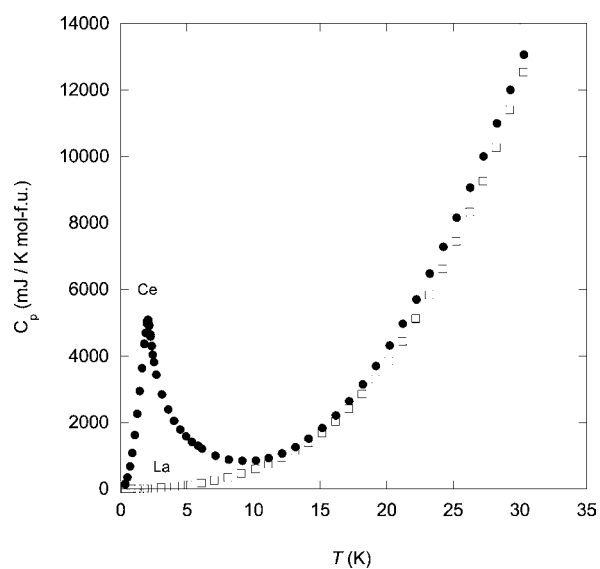followed by a sharp peak at 2 K signifying a phase transition that closely coincides with θ_W obtained from fits to the magnetic susceptibility data. Fits of C_p/T vs T^2 data for LaCu$_2$(Al,Si)$_5$ and CeCu$_2$(Al,Si)$_5$ were performed to extract the β and γ coefficients. The values for β and γ obtained from these fits for LaCu$_2$(Al,Si)$_5$ [CeCu$_2$(Al,Si)$_5$] were found to be equal to 0.442 mJ/mol K^4 [0.457 mJ/mol K^4] and 12.34 mJ/mol K^2 [24.53 mJ/mol K^2]. The Debye temperature for both analogues was calculated using the formula, $\theta_D{}^3 = (234 \cdot n \cdot k_B)/\beta$ where n is the density and k_B is Boltzmann's constant. The calculated Debye temperatures for LaCu$_2$(Al,Si)$_5$ and CeCu$_2$(Al,Si)$_5$ are 163 and 162 K, respectively. Because the Debye temperatures for LaCu$_2$(Al,Si)$_5$ and CeCu$_2$(Al,Si)$_5$ are nearly equivalent, the magnetic heat capacity divided by temperature (C_m/T) for CeCu$_2$(Al,Si)$_5$ (Figure 8) could be determined by subtraction of the phonon contribution to heat capacity by the non-
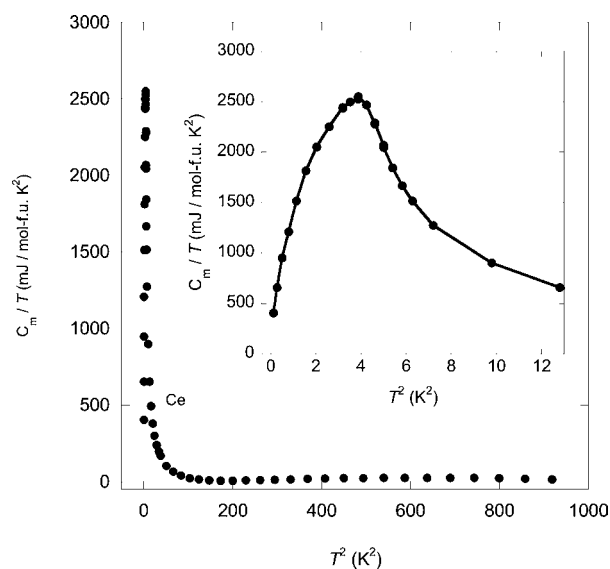
Figure 8. Plot of magnetic heat capacity divide by temperature (C_m/T) vs T^2 for $CeCu_2(Al,Si)$, where C_m is the magnetic contribution to the specific heat determined by subtracting the $C_p(T)$ of $LaCu_2(Al,Si)_5$. The inset serves to highlight the transition.

magnetic $LaCu_2(Al,Si)_5$ analogue. The magnetic entropy, S_{mag}, as a function of temperature was determined by integrating C_m/T and is shown in Figure 9. The expected entropy, $S_{mag} =$
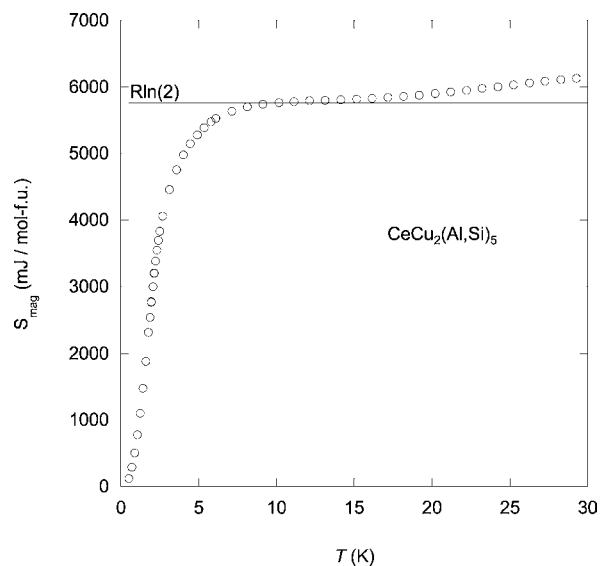

Figure 9. Magnetic entropy (S_{mag}) as a function of temperature (T). Rln2 is indicated by the line.

$Rln(2S + 1)$ with $S = 1/2$, is completely recovered from the lowest temperatures measured to the onset of the transition, around 10 K. It is interesting to again note that the onset of the deviation of the magnetic susceptibility data for $CeCu_2(Al,Si)_5$ from Curie–Weiss behavior occurred at around 10 K (This can be seen as the red curve in Figure 3.). With the entropy associated with the transition in C_m being in good agreement with the entropy expected for a magnetic transition, it is reasonable to assert that the transition at 2 K is due to a magnetic ordering of Ce atoms. Furthermore, the positive θ_W and the nice scaling of the field-dependent magnetization by

the subtraction of 2 K to the temperature also suggest that this transition is ferromagnetic in nature (Figure 5a and b).

CONCLUSIONS

Single crystals of $LaCu_2(Al,Si)_5$ and $CeCu_2(Al,Si)_5$ were grown by the flux growth technique and subsequent phase pure polycrystalline samples were prepared by arc melting of the constituent elements in stoichiometric ratios and annealing. Single crystals of both $LaCu_2(Al,Si)_5$ and $CeCu_2(Al,Si)_5$ were characterized by single crystal X-ray diffraction and composition was determined by EDS. The polycrystalline samples were characterized by powder X-ray diffraction, using both in-house equipment and the synchrotron source at APS. We have shown that the magnetic susceptibility of $CeCu_2(Al,Si)_5$ is paramagnetic down to the lowest temperature measured, $T = 2.25$ K. The Curie–Weiss analysis and magnetization scaling suggest that magnetic correlations for $CeCu_2(Al,Si)_5$ become relevant at 10 K and are likely ferromagnetic ($\theta_W = 2$ K). This is supported by the heat capacity data where a transition was observed to peak at 2 K. In addition, the low-temperature transport behavior of $CeCu_2(Al,Si)_5$ is consistent with incoherent Kondo scattering interactions at high temperatures. Thus, our data indicate that $CeCu_2(Al,Si)_5$ has a somewhat enhanced carrier mass, $\gamma \sim 25$ mJ/mol K^2, and likely undergoes a ferromagnetic transitions at 2 K, placing it among only a handful of ferromagnetic Ce compounds.[16,38−40] The occurrence of ferromagnetism in a Ce compound displaying distinct features of Kondo screening at higher temperatures may be indicating an underscreened or undercompensated Kondo lattice, which has been predicted and experimentally shown to result in the formation of a singular Fermi liquid. Measurement of the electrical transport of $CeCu_2(Al,Si)_5$ at lower temperature is thus of interest to explore this possibility.[41−44]

ASSOCIATED CONTENT

Ⓢ Supporting Information
Single crystal and powder X-ray diffraction CIFs for the $LaCu_2(Al,Si)_5$ and $CeCu_2(Al,Si)_5$ compounds. This material is available free of charge via the Internet at http://pubs.acs.org.

AUTHOR INFORMATION

Corresponding Author
*E-mail: jchan@lsu.edu. Telephone: (225) 578-2695. Fax: (225) 578-3458.

REFERENCES

(1) Petrovic, C.; Movshovich, R.; Jaime, M.; Pagliuso, P. G.; Hundley, M. F.; Sarrao, J. L.; Fisk, Z.; Thompson, J. D. *Europhys. Lett.* **2001**, *53*, 354−359.
(2) Petrovic, C.; Pagliuso, P. G.; Hundley, M. F.; Movshovich, R.; Sarrao, J. L.; Thompson, J. D.; Fisk, Z.; Monthoux, P. *J. Phys.: Condens. Matter* **2001**, *13*, L337.
(3) Bauer, E.; Pillmayr, N.; Gratz, E.; Gignoux, D.; Schmitt, D.; Winzer, K.; Kohlmann, J. *J. Magn. Magn. Mater.* **1988**, *71*, 311−317.

(4) Macaluso, R. T.; Nakatsuji, S.; Lee, H.; Fisk, Z.; Moldovan, M.; Young, D. P.; Chan, J. Y. *J. Solid State Chem.* **2003**, *174*, 296−301.

(5) Kishimoto, Y.; Kawasaki, Y.; Ohno, T. *Phys. Lett. A* **2003**, *317*, 308−314.

(6) Fisk, Z; Sarrao, J L; Smith, J L; Thompson, J D *Proc. Natl. Acad. Sci. U.S.A.* **1995**, *92*, 6663−6667.

(7) Fisk, Z. *Science* **2007**, *318*, 1559−1560.

(8) Macaluso, R. T.; Nakatsuji, S.; Kuga, K.; Thomas, E. L.; Machida, Y.; Maeno, Y.; Fisk, Z.; Chan, J. Y. *Chem. Mater.* **2007**, *19*, 1918−1922.

(9) Hegger, H.; Petrovic, C.; Moshopoulou, E. G.; Hundley, M. F.; Sarrao, J. L.; Fisk, Z.; Thompson, J. D. *Phys. Rev. Lett.* **2000**, *84*, 4986.

(10) Macaluso, R. T.; Millican, J. N.; Nakatsuji, S.; Lee, H.-O.; Carter, B.; Moreno, N. O.; Fisk, Z.; Chan, J. Y. *J. Solid State Chem.* **2005**, *178*, 3547−3553.

(11) Cordier, G.; Dietrich, C.; Friedrich, T. *Z. Kristallogr.* **1996**, *211*, 627−628.

(12) Cho, J. Y.; Millican, J. N.; Capan, C.; Sokolov, D. A.; Moldovan, M.; Karki, A. B.; Young, D. P.; Aronson, M. C.; Chan, J. Y. *Chem. Mater.* **2008**, *20*, 6116−6123.

(13) Thomas, K. R.; Cho, J. Y.; Millican, J. N.; Hembree, R. D.; Moldovan, M.; Karki, A.; Young, D. P.; Chan, J. Y. *J. Cryst. Growth* **2010**, *312*, 1098−1103.

(14) Menard, M. C.; Drake, B. L.; McCandless, G. T.; Thomas, K. R.; Hembree, R. D.; Haldolaarachchige, N.; DiTusa, J.; Young, D. P.; Chan, J. Y. *Eur. J. Inorg. Chem.* **2011**, *26*, 3909−3919.

(15) Cho, J. Y.; Capan, C.; Young, D. P.; Chan, J. Y. *Inorg. Chem.* **2008**, *47*, 2472−2476.

(16) Drake, B. L.; Kangas, M. J.; Capan, C.; Haldolaarachchige, N.; Xiong, Y. M.; Adams, P. W.; Young, D. P.; Chan, J. Y. *J. Phys.: Condens. Matter* **2010**, *22*, 426002.

(17) Romaka, V. A.; Grin, Y. N.; Yarmolyuk, Y. P. *Ukr. Fiz. Zh.* **1983**, *28*, 1095−1097.

(18) Drake, B. L.; Capan, C.; Cho, J. Y.; Nambu, Y.; Kuga, K.; Xiong, Y. M.; Karki, A. B.; Nakatsuji, S.; Adams, P. W.; Young, D. P.; Chan, J. Y. *J. Phys.: Condens. Matter* **2010**, *22*, 066001.

(19) Gout, D.; Benbow, E.; Gourdon, O.; Miller, G. J. *Inorg. Chem.* **2004**, *43*, 4604−4609.

(20) Tobash, P. H.; Ronning, F.; Thompson, J. D.; Bobev, S.; Bauer, E. D. *J. Solid State Chem.* **2010**, *183*, 707−711.

(21) Canfield, P. C.; Fisk, Z. *Philos. Mag. B* **1992**, *65*, 1117−23.

(22) Altomare, A.; Burla, M. C.; Camalli, M.; Luca, G. L.; Gaicovazzo, C.; Guagliardi, A.; Moliterni, A. G. G.; Polidori, G.; Spagna, R. *J. Appl. Crystallogr.* **1999**, *32*, 115.

(23) Sheldrick, G. M. *Acta Crystallogr., Sect. A* **2008**, *64*, 112−122.

(24) Wang, J.; Toby, B. H.; Lee, P. L.; Ribaud, L.; Antao, S. M.; Kurtz, C.; Ramanathan, M.; Von Dreele, R. B.; Beno, M. A. *Rev. Sci. Instrum.* **2008**, *79*, 085105.

(25) Larson, A. C.; Von Dreele, R. B. *Los Alamos National Laboratory Report LAUR* **2004**, 86−748.

(26) Toby, B. H. *J. Appl. Crystallogr.* **2001**, *34*, 210−213.

(27) Bobev, S.; Tobash, P. H.; Fritsch, V.; Thompson, J. D.; Hundley, M. F.; Sarrao, J. L.; Fisk, Z. *J. Solid State Chem.* **2005**, *178*, 2091−2103.

(28) Zarechnyuk, O. S.; Kripyakevich, P. I.; Gladyshevskii, E. I. *Kristallografiya* **1964**, *9*, 835−838.

(29) Kim, S. M.; Buyers, W. J. L.; Lin, H.; Bauer, E. *Z. Phys. B* **1991**, *84*, 201−203.

(30) Bodak, O. I.; Gladyshevskii, E.; Kripyakevich, P. I. *Inorg. Mater. (USSR)* **1966**, *2*, 1861−1864.

(31) Landelli, A. *J. Less-Common Met.* **1983**, *90*, 121−126.

(32) Pecharsky, V. K.; Gschneidner, J. K. A. *Int. J. Refrig.* **2006**, *29*, 1239−1249.

(33) Foldeaki, M.; Chahine, R.; Bose, T. K. *J. Appl. Phys.* **1995**, *77*, 3528−3537.

(34) McMichael, R. D.; Ritter, J. J.; Shull, R. D. *J. Appl. Phys.* **1993**, *73*, 6946−6948.

(35) Das, P. K.; Kumar, N.; Kulkarni, R.; Thamizhavel, A. *Phys. Rev. B* **2011**, *83*, 134416.

(36) Pikul, A. P.; Kaczorowski, D.; Rogl, P.; Grin, Y. *Phys. Status Solidi B* **2003**, *236*, 364−367.

(37) Babizhetskyy, V.; Guerin, R.; Isnard, O.; Hiebl, K. *J. Solid State Chem.* **2003**, *172*, 265−276.

(38) Macaluso, R. T.; Wells, D. M.; Sykora, R. E.; Albrecht-Schmitt, T. E.; Mar, A.; Nakatsuji, S.; Lee, H.; Fisk, Z.; Chan, J. Y. *J. Solid State Chem.* **2004**, *177*, 293−298.

(39) Sidorov, V. A.; Bauer, E. D.; Lee, H.; Nakatsuji, S.; Thompson, J. D.; Fisk, Z. *Phys. Rev. B* **2005**, *71*, 094422.

(40) Thomas, E. L.; Gautreaux, D. P.; Lee, H. O.; Fisk, Z.; Chan, J. Y. *Inorg. Chem.* **2007**, *46*, 3010−3016.

(41) Sacramento, P. D.; Schlottmann, P. *J. Phys.: Condens. Matter* **1991**, *3*, 9687−9696.

(42) Gan, J.; Coleman, P.; Andrei, N. *Phys. Rev. Lett.* **1992**, *68*, 3476−3479.

(43) Coleman, P.; Pepin, C. *Phys. Rev. B* **2003**, *68*, 220405(R).

(44) Manyala, N.; DiTusa, J. F.; Aeppli, G.; Ramirez, A. P. *Nature* **2008**, *454*, 976−980.